forests

A 1640-year Vegetation and Fire History of the Lake Haixihai Catchment in Northwestern Yunnan, Southwest China

Qian Shi[1], Caiming Shen[1*], Hongwei Meng[1], Linpei Huang[1], Qifa Sun[1]

[1] Yunnan Key Laboratory of Plateau Geographical Processes and Environmental Changes, Faculty of Geography, Yunnan Normal University, Kunming 650500, China
* Correspondence: caiming_shen@ynnu.edu.cn

Abstract: Vegetation and fire archives of the late Holocene are essential for understanding the importance of natural and anthropogenic forcings on past and future vegetation successions and climate changes. Here we present a 1640-year record of vegetation and fire history of the Lake Haixihai catchment in northwestern Yunnan, southwest China. Pollen and charcoal analyses as well as XRF (X-Ray fluorescence) analysis of lacustrine sediments from Lake Haixihai were employed to reveal its regional vegetation, forest fire and soil erosion intensity changes over the last 1640 years. The results show their significant changes attributed to both climatic conditions and human activities: The lake catchment witnessed the densest forests (including pine and hemlock forests, and evergreen broadleaved forests) and the weakest soil erosion of the last 1640 years as well as relatively frequent forest fires at 380-880 AD, when vegetation succession, forest fire, and soil erosion were mainly driven by natural forcings, i.e., climatic conditions. A significant and abrupt drop in forest density, minor changes in abundance of forest components, and gradually strengthening soil erosion occurred at the transition from 880 to 1040 AD, when anthropogenic forcings such as the development of agriculture and systematic deforestation gradually became dominant ones driving vegetation succession and soil erosion. After this transition, forest density and soil erosion intensity never returned to the level before 880 AD, implying that modern landscape in the lake catchment was already established approximately at as early as ca. 1040 AD. No significant changes in forest component and density as well as forest fire and soil erosion occurred until 1940 AD. The most frequent forest fires, the strongest soil erosion, and low forest density after 1940 AD might be attributed partially to climatic conditions and partially to extensive deforestation around 1960 AD.

Keywords: pollen; charcoal; vegetation succession; forest fire; soil erosion

1. Introduction

The period of the last 2000-year, when global environments were affected by both natural and anthropogenic forcings, is the critical stage for understanding the impact of anthropogenic forcing on environmental changes in the context of natural variability [1]. Among a lot of environmental parameters, vegetation or land cover and fire or biomass burning are two important parameters. Previous studies have shown that spatial and temporal patterns of vegetation and fire driven by natural and anthropogenic forcings are significantly different among various regions of the world, China, and even Yunnan over the last two millennia [2-5]. Obviously, more records are needed to develop a detailed picture of regional vegetation changes and fire activities so that we may understand their global temporal and spatial patterns and dominant driving forcings over the last two millennia.

As one of the most biodiverse regions in the world, the northwestern Yunnan, i.e., the southeastern margin of the Tibetan Plateau, is sensitive to climate change and human activities [6,7]. In the past decades, a lot of studies were carried out to reveal regional vegetation and fire histories in Yunnan. However, most of fossil records used in these studies were mainly from nine large lakes in Yunnan, i.e., Lakes Lugu [8], Erhai [9],

Chenghai [10], Qilu [11], Xingyun [12], Fuxian [13], Dianchi [14], Yangzonghai [15], and Yilong [16], the huge pollen and charcoal source areas for these large lakes bring about more difficulties and uncertainties in the interpretation of fossil pollen and charcoal records in terms of regional vegetation and forest fires rather than small-medium size lakes [17]. Although some pollen records were from small-medium size lakes such as Lakes Xihu [18], Tiancai [19], Yunlong Tianchi [20] and Tengchong Qinghai [21], these studies focused on long-term vegetation succession and fire history in the last deglaciation and Holocene. Therefore, we selected a medium-size lake, Lake Haixihai, in the Lake Erhai basin, the center of economy and culture during the historical times in Yunnan, as our research object to emphasize vegetation succession and forest fire history during the past 1640 years.

In this study, we used pollen/charcoal analysis and XRF analysis of lacustrine sediments from Lake Haixihai to reveal the changes of vegetation, forest fire, and soil erosion intensity over the last 1640 years in the lake catchment, and then to determine the roles of natural and anthropogenic forcings in driving these changes.

2. Location and Setting

Lake Haixihai (26°16′-26°18′N, 99°57′-99°59′E, 2130 m above sea level) (Figure 1a, b) is located in northwestern Yunnan, Southwest China. It is a medium-size lake with an area of 2.6 km^2 (Figure 1d). This lake's maximum length and width are 3.6 and 1.5 km, and its average and maximum water depths are 10 and 21 m (measured value in 2019). As one important water source in the upper reaches of large Lake Erhai, the lake water finally flows to Lake Erhai through Mici River, Lake Cibi, Fengyu River and Miju River [22]. Climatologically, the catchment of Lake Haixihai has a subtropical monsoon climate. Observational data of 1981-2010 at Eryuan meteorological station, which is located at 24 km south of Lake Haixihai, shows a mean annual precipitation of 714 mm, in which 643 mm (over 90%) is concentrated in rainy season from May to October mostly brought about by the South Asian summer monsoon, exhibiting obvious characteristics of wet and dry seasons (Figure 2). The mean annual temperature is 14.9℃, with the warmest temperature of 20.5℃ in July and the coldest temperature of 7.4 ℃ in January. The mean annual temperature is 13.9 ºC, with average January and July temperatures of 7 and 20 ºC (Figure 2). Geologically, the bedrock of the Lake Haixihai catchment mainly includes limestone, sandstone, and mudstone [23].

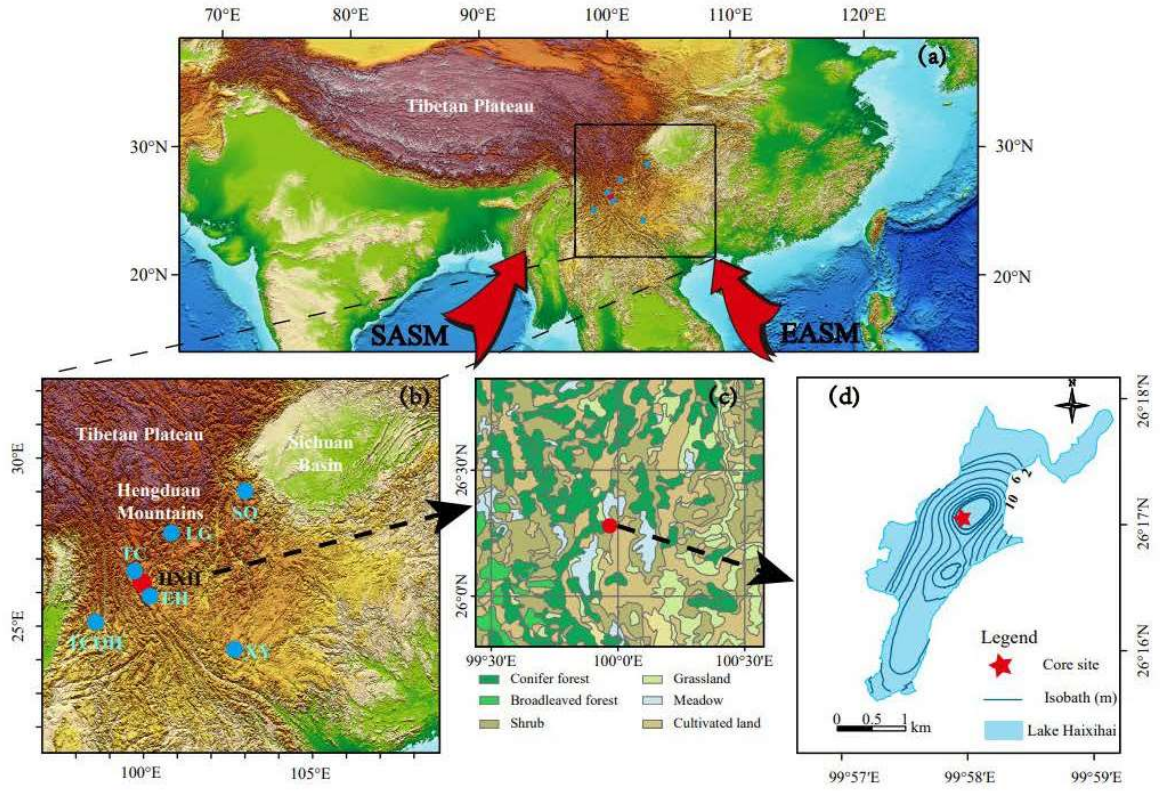


Figure 1. Topography and location of the study site and records cited in the study. (a) map showing locations of the study site, the arrows display the atmospheric circulation systems (SASM, South Asian Summer Monsoon; EASM, East Asian Summer Monsoon); (b) topography and locations of the study site (red dot) and records cited in the study (blue dot), including Lakes Lugu (LG), Chenghai (CH), Erhai (EH), Tiancai (TC), Yunlong Tianchi (YLTC), Tengchong Qinghai (TCQH), Dianchi (DC), Yangzonghai (YZ), Fuxian (FX), Xingyun (XY), Qilu (QL), and Yilong (YL) as well as Baihai wetland (BH); (c) distribution of vegetation within 50 km of the Lake Haixihai catchment [26]; (d) the coring location of core HXH-1 in Lake Haixihai.

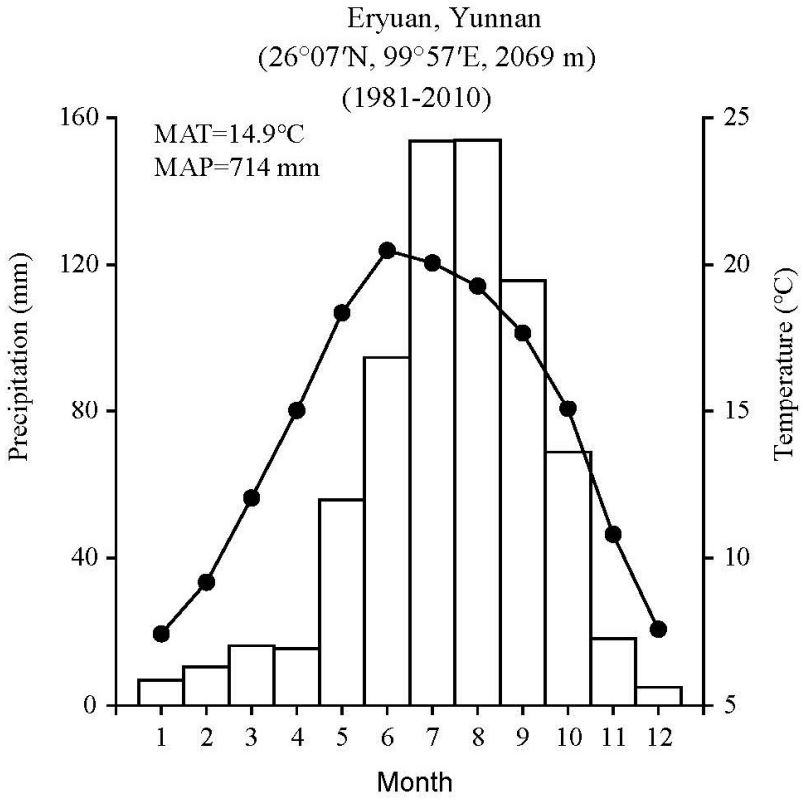


Figure 2. Monthly mean precipitation and temperature from 1981 to 2010 at Eryuan meteorological station (ca. 20 km south of Lake Haixihai) in near northwestern Yunnan, China.

Modern vegetation in the catchment of Lake Haixihai and its adjacent regions is dominated by forests, shrubs, grasslands, meadows, and cultivated lands (Figure 1c). *Pinus yunnanensis* forest is the dominant conifer one, in which *Pinus yunnanensis* is often accompanied by evergreen and deciduous broadleaved trees such as *Castanopsis delavayi*, *Cyclobalanopsis delavayi*, *Alnus nepalensis*, and *Quercus variabilitis*; semi-humid evergreen broadleaved forest is the dominant broadleaved one, in which *Cyclobalanopsis glaucoides, C. delavayi*, *Castanopsis delavayi*, and *C. orthocantha* are its major components, and some deciduous broadleaved trees such as *Celtis yunnanensis*, *Pistacia chinensis*, *Albizia mollis*, *Alnus nepalensis*, *Populus yunnanensis, Platycarya strobilacea, Querscus acutissima, Q. variabilis,* and *Q. aliena* are main accompanying elements [24]. In the adjacent mountainous slopes, e.g., west slopes of Cangshan Mountain, occurs the altitudinal zonation of vegetation. The zone below 2500 m is occupied by *Pinus yunnanensis* forest; the zone between 2500 and 2900 m is dominated by evergreen broadleaved forest and *Pinus armandii* forest; the 2900-3300 m zone is occupied by mixed forest of *Tsuga dumosa* and broadleaved trees; the zone of 3300-3500 m is dominated by *Abies delavayi-Rhododendron simsii* forest; Above 3500 m occurs subalpine meadow [25]. In the catchment of Lake Haixihai, shrubs are dominated by *Vaccinium bracteatum, Myrica nan,* and *Rhododendron simsii* formations; grasslands consist mainly of *Arundinella setosa* and *A. hookeri; Festuca ovina* and *Deyeuxia pyramidalis* as well as forb formations are common meadows. Cultivated lands are occupied by deciduous orchards such as walnut and apple and food crops such as wheat, corn and rape [26].

3. Materials and methods

In 2019, a 290-cm sediment core (core HXH-1) was taken from the center of Lake Haixihai (26°17′N, 99°58′E) under 20.7 m of water (Figure 1d) using the above-water platform and the Austrian UWITEC piston sampling equipment. The terrestrial plant residues

were used for AMS ^{14}C dating. The dating of 1 leaf sample and 2 wood chip samples were conducted at the Beta Laboratory in the United States.

Twenty-nine elements (Al-U) and magnetic susceptibility of core HXH-1 were continuously scanned and analyzed at 5 mm interval, 10 mm width, and 30 s duration by a Dutch Avaatech XRF scanner. The analysis was conducted at Yunnan Key Laboratory of Plateau Geographical Processes and Environmental Changes, Yunnan Normal University. Elemental data as elemental counts per second (cps) and low-frequency magnetic susceptibility (χ_{lf}) in the core sediment were acquired through the Avaatech software. Although the element concentrations obtained by XRF scanning are not absolute element concentrations, they can reflect the changes in the relative contents of elements well [27]. Al, Si, K, Fe and Ti are common terrigenous detrital tracer elements [28-31], Ca element is lake biogenic or terrigenous clastic origin [30, 32], and Ti was also used as the proxy of monsoonal precipitation and vegetation density in monsoon Asia [33-35], thus elements of Al, Si, K, Fe, Ti and Ca are major elements with obvious environmental significance and high reliability [36-38]. Principal component analysis (PCA) of major elemental data was employed to assist the environmental interpretation of elemental data.

The core was sampled at the 6-cm interval (a total of 49 samples) for pollen analysis. Pollen samples of 1 cc were processed using standard methods involving HCl, KOH, HF, and acetolysis treatment [39]. Pollen residues were finally washed by sieving through 7 μm meshes. Pollen and charcoal were extracted simultaneously, and their concentrations and influx values were estimated with tables containing a known quantity of *Lycopodium* spores as exotic markers [40]. The total pollen influx values in this study were used as a proxy of vegetation density [41-43]. The identification and counting of pollen and charcoal were carried out under the Olympus optical microscope with a magnification of 400 times. More than 500 pollen grains were counted at each level, and average of 49 samples was 573 grains. The identification of charcoal is based on the grading method [44]. According to the longest axis length of the charcoal particle, the charcoals were assigned into three groups, i.e., <50, 50-100, and >100 μm [44]. Pollen percentages were calculated based on a sum of all terrestrial plant pollen. Pollen percentage and influx diagrams of selected pollen types were plotted using Tilia software. Pollen zones were divided in terms of cluster analysis on the pollen percentage data of major arboreal pollen types [45]. PCA of major arboreal pollen percentage data was also performed to help the vegetational interpretation of pollen spectra and zones. PCA was conducted in Canoco 5.

4. Results

4.1. Stratigraphy and chronology of core HXH-1

The 290-cm core from Lake Haixihai is mainly composed of silts. Three lithological units can be recognized from the sediment color and low-frequency magnetic susceptibility (Figure 3). The 290-203 cm unit contains dark gray silts and low magnetic susceptibility. The unit of 203-65 cm consists of reddish-brown silts with high magnetic susceptibility. The 65-0 cm unit contains grayish silts interbedded with reddish brown silt layers, and sediments in this unit have high magnetic susceptibility and significantly oscillations, especially the upper 30 cm.

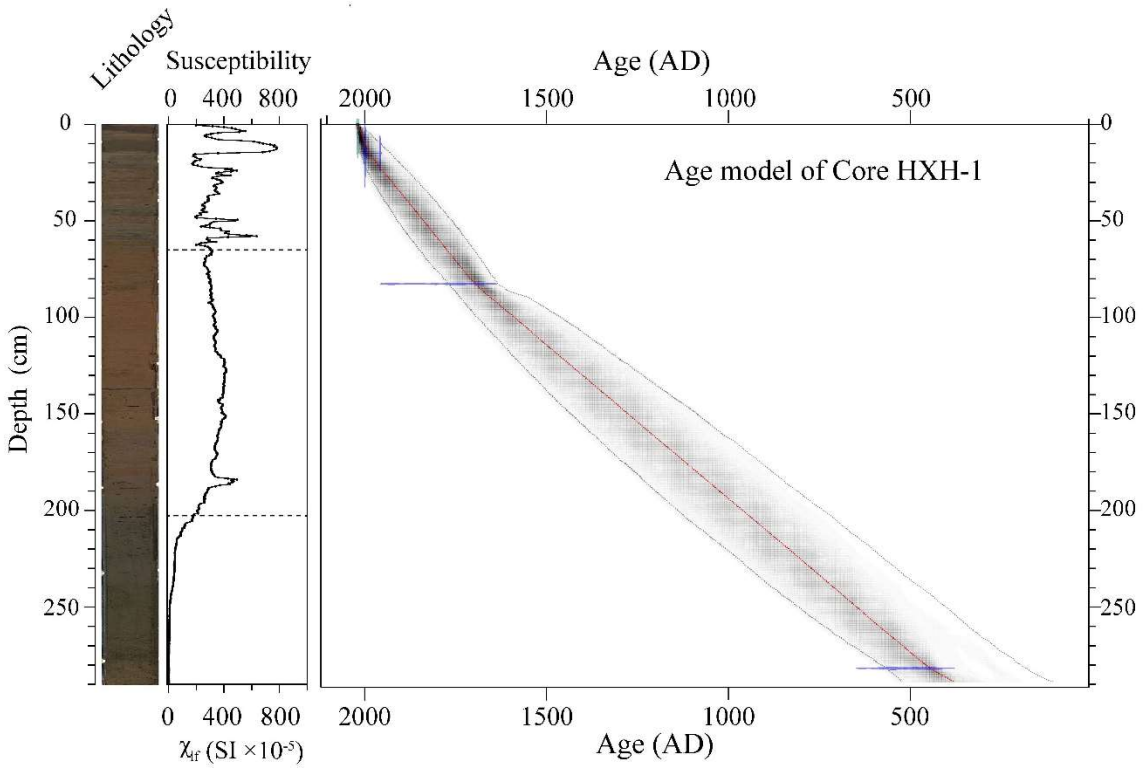


Figure 3. Lithology, magnetic susceptibility, and age-depth model for core HXH-1 from Lake Haixihai.

In order to avoid the reservoir effect on the radiocarbon dating, we selected the terrestrial plant tissues as the dating materials. Table 1 shows the dating results of one leaf sample and two woody chip samples. Two ^{14}C ages at 83 and 283 cm were calibrated using IntCal 20 [46], and one ^{14}C age at 15 cm was converted to calendar years using a combination of IntCal20 and NHZ3 calibration curves [47,48]. The radiocarbon date of leaf sample at 15 cm is -770±50 ^{14}C yr BP, and its calibrated age with 1σ error range is 1970-2010 AD with a median age of 1990 AD. This age is very close to that (~1984.3±3.0 AD at 14.5 cm) estimated by the constant rate of supply (CRS) model based on the measurement of ^{210}Pbex and ^{137}Cs radionuclide activities of a 37.5-cm short core in the same lake [49], implying that the lake has no or negligible reservoir effect. After the top age was set as 2019 AD, the Bayesian depth-age [50] was finally established using three calibrated ages and the top age.

Table 1. AMS ^{14}C dating results for core HXH-1 from Lake Haixihai.

Lab. ID	Depth (cm)	Dating material	^{14}C age (yr BP)	pMC[a]	Calibrated age (AD)
Beta-594071	15	Leaves		110.06±0.41	1996-2000[b]
Beta-594072	83	Wood	150±30	98.15±0.37	1670-1780[c]
Beta-594073	283	Charcoal	1550±30	82.45±0.31	430-590[c]

[a]pMC=percentage of modern carbon. [b]Age was calibrated by the percentage of modern carbon using high probability density range method. [c]Age was calibrated by conventional radiocarbon age using high probability density range method.

4.2. XRF core scanning of major elements

The major elements of core HXH-1 core were characterized by significant changes in their concentrations (Figure 4). Among six major elements, Ca and Fe concentrations are the highest, Ti, K and Si concentrations are in the second place, and Al concentration is the least. The elemental profiles of this core can be divided into three units.

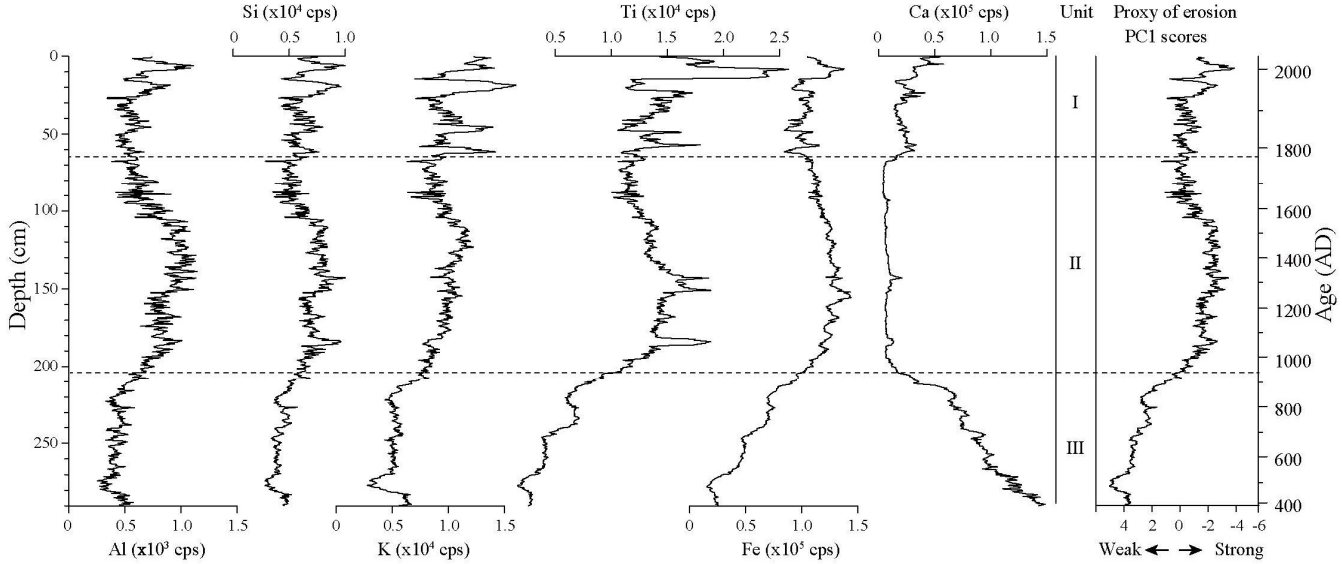


Figure 4. Concentrations of six major elements obtained by XRF scanning and their PC1 scores as the proxy of soil erosion intensity for core HXH-1 from Lake Haixihai.

Unit III (290-204 cm; 380-940 AD): This unit is marked by low Al, Si, and K concentrations, and high Ca concentration. Fe and Ti concentrations increase from the bottom to the top of this unit.

Unit II (204-65 cm; 940-1800 AD): This unit is characterized by high Al, Si, K, Fe, and Ti concentrations, and low Ca concentration.

Unit I (65-0 cm; 1800 AD to the present): This unit is marked by large variabilities in concentrations of six major elements. In this unit, Ca concentration is higher than unit II but lower than unit I.

As shown by Figure 4, concentrations of Al, Si, K, Fe, and Ti exhibit approximate covariations in core HXH-1, whereas Ca concentration show a opposite trend. The correlation analysis between Ca and other elements further demonstrates their relationships (Figure 5a). A positive correlation statistically significant at $p<0.001$ level occurs among Al, Si, K, Fe, and Ti elements, and a negative correlation statistically significant at $p<0.001$ level exists between Ca and other five elements respectively. The result of PCA on concentration data of six major elements also shows the same fact (Figure 5b). The broken stick model indicates that only PC1 has statistical significance. The PC1 explains 81.8% of the total variance in this dataset. On the PC1 axis, Ca is at right side (positive loading), whereas the others are at left side (negative loading), indicating the two groups of elements are from completely different sources. Since Al, Si, K, Fe and Ti are common terrigenous detrital tracer elements, Ca is from endogenously biogenic origin of the lake rather than terrigenous clastic origin. It is evident that the PC1 of elements reflects relative abundance of exogenous and endogenous substances in lake sediments, i.e., the erosion intensity of the lake catchment. The PC1 of elements can thus be used as a proxy of soil erosion intensity in the Lake Haixihai catchment. As PC1 sample scores become small, the soil erosion intensity reinforces.

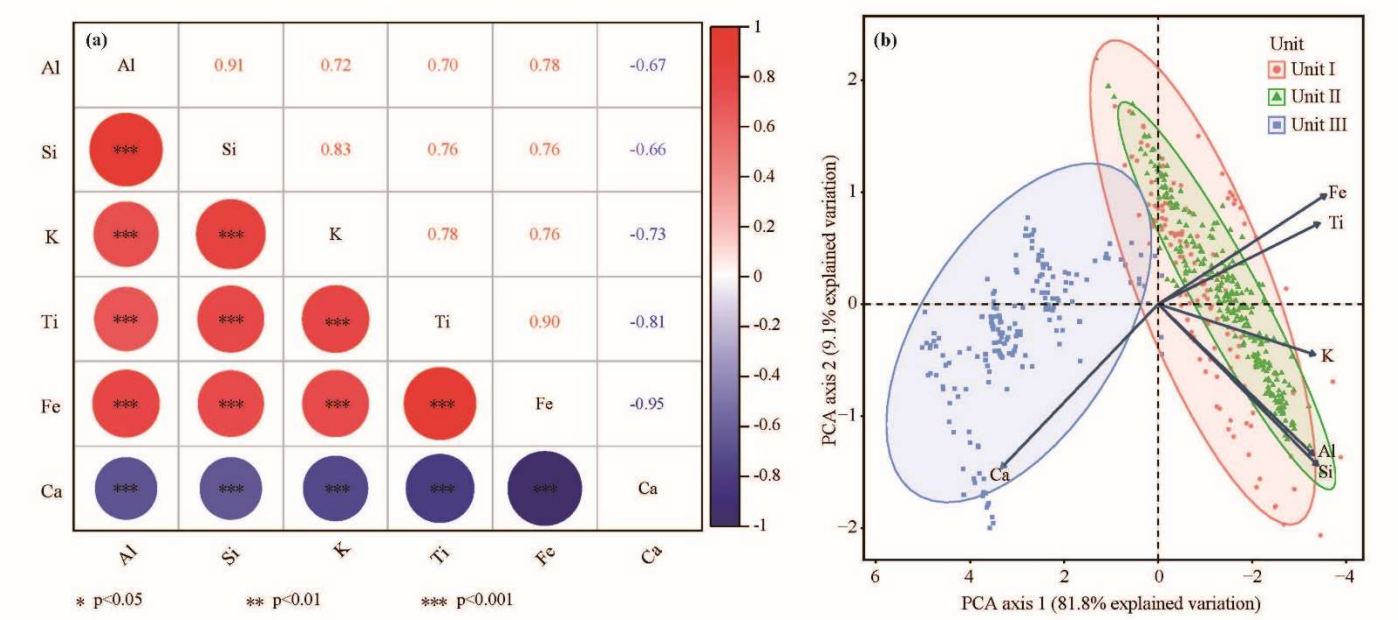


Figure 5. Element correlations (a) and biplot of PCA on the concentration data of six major elements (b) for core HXH-1 from Lake Haixihai.

As shown by Figures 4 and 5b, the soil erosion intensity of the last 1640 years experienced three-phase changes. In the phase III (corresponding to unit 3 of elemental profiles) at 380-940 AD, the weakest erosion of the last 1640 years occurred at 380-570 AD (290-263 cm), and the erosion enhanced nonlinearly. The phase II witnessed a continuously strengthening erosion from 940 to 1090 AD, a persistent and strong erosion between 1090 and 1560 AD, and relative weak erosion at 1560-1770 AD. During the phase I, above relative weak erosion continued until 1940 AD, and then the erosion dramatically became as strong as that at 1090-1560 AD; after a brief reversal in 1980s AD, the erosion strengthened to be the strongest around 2000 AD, and kept strong until the present.

4.3. Pollen/charcoal record

Pollen spectra from Lake Haixihai are dominated by arboreal pollen, mainly including coniferous tree pollen such as *Abies*, *Abies/Picea*, *Pinus* and *Tsuga*, evergreen and deciduous broadleaved tree pollen such as *Castanopsis/Lithocarpus*, *Cyclobananopsis*, evergreen *Quercus*, deciduous *Quercus*, *Alnus*, *Betula*, *Juglans*, *Salix*, and Anacardiaceae, shrub pollen such as Rosaceae, Elaeagnaceae, and Ericaceae. Herbaceous pollen contains mainly Poaceae, *Artemisia*, Cyperaceae Asteraceae, Chenopodiaceae, and *Polygonum*. Pollen/charcoal record is divided into three pollen zones based on the result of CONISS analysis of pollen percentage data of arboreal pollen types with the average of pollen percentage more than 1% (Figure 6).

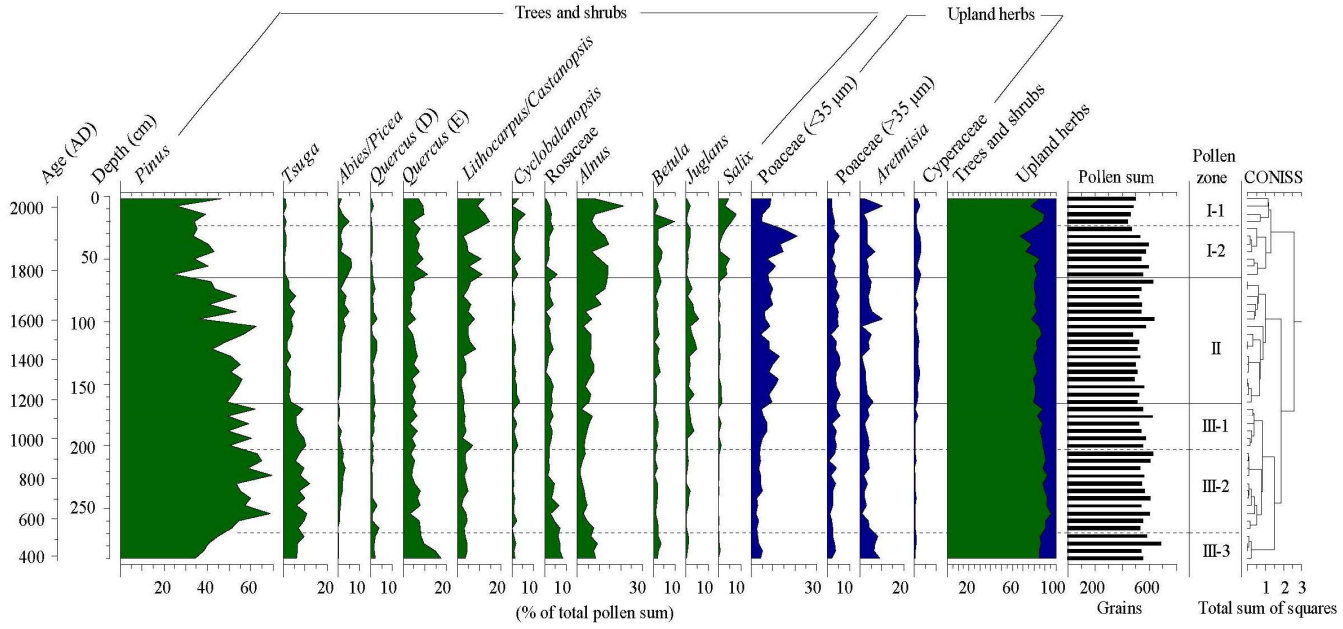


Figure 6. Pollen percentage diagram of selected pollen taxa for core HXH-1 from Lake Haixihai.

Zone III (290-166 cm; 380-1180 AD): This zone is characterized by the highest arboreal and the lowest herbaceous pollen percentages of the entire core (86.8 and 13.2%, the averages of pollen spectra in the zone, the same below) (Figure 3). Among arboreal pollen, *Pinus* is the most abundant (52.3%), followed by *Tsuga* (7.6%), *Quercus* (E) (6.6%), and *Alnus* (4.3%). Herbaceous pollen mainly includes Poaceae (6.8%) and *Artemisia* (3.8%). Pollen influx diagram (Figure 7) shows that total pollen influx values in this zone are the highest in the whole core with an average of 9154 grains cm^{-2} a^{-1}. This zone can be further divided into 3 subzones. Subzone III-2 is distinguished from subzone III-1 by a significant increase of *Pinus* pollen percentages from 40.3% to 58.3%, a marked decrease of *Quercus* (E), *Alnus*, and *Artemisia* pollen percentages, and a dramatic rise in the pollen influx values from less than 10000 grains cm^{-2} a^{-1} to more than 20000 grains cm^{-2} a^{-1}. Subzone III-3 is separated from subzone III-2 by a decrease of Pinus pollen percentages and an abrupt decline in total pollen influx values from 24765 to 1351 grains cm^{-2} a^{-1}. This zone has relatively high total charcoal influx values (26093 particles cm^{-2} a^{-1}), and the highest >100 μm charcoal influx values (665 particles cm^{-2} a^{-1}) occur in the subzone III-2.

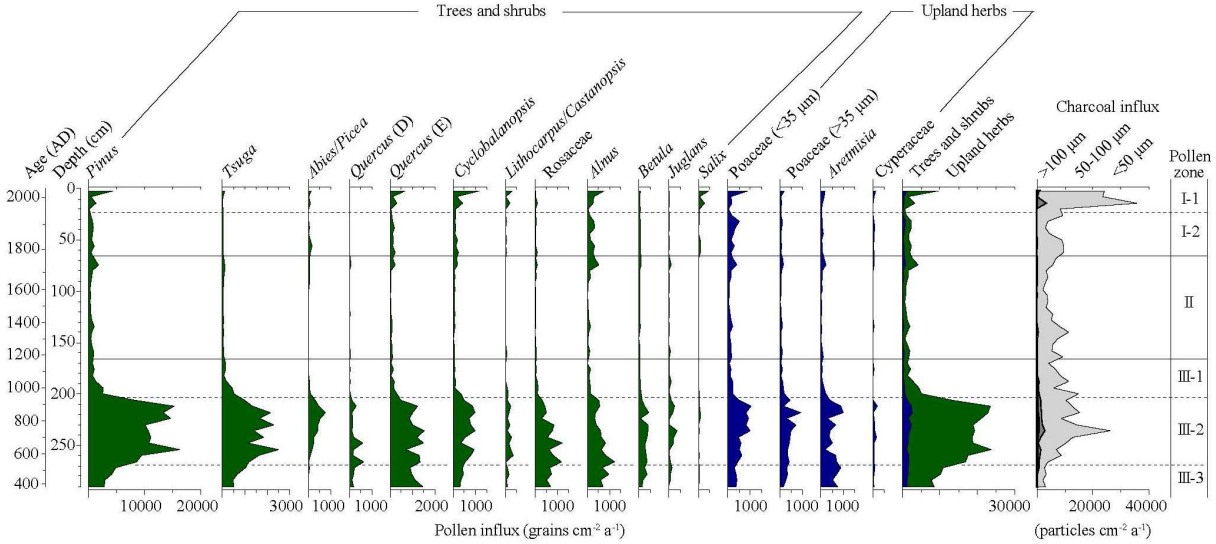


Figure 7. Pollen influx diagram of selected pollen taxa for core HXH-1 from Lake Haixihai.

Zone-II (166-65 cm; 1180-1770 AD): This zone is marked by continuous declines of *Pinus* pollen percentages, a distinct increase of herbaceous pollen percentages, and the minima of total pollen influx values. In this zone, pollen percentages of *Tsuga* and *Quercus* (E) also decrease beside *Pinus*. Other arboreal pollen such as *Cyclobalanopsis*, *Alnus* and *Juglans* increases. Among herbaceous pollen, Poaceae pollen increases from 6.8% to 12.6%, and *Artemisia* pollen is common (about 3.8%). Total pollen influx values decrease significantly (1525 grains cm^{-2} a^{-1}) with a small range (654 to 4399 grains cm^{-2} a^{-1}) in this zone. The total charcoal influx values (5548 particles cm^{-2} a^{-1}) also decline to be its minima.

Zone I (65-0 cm, 1770 AD to the present): This zone is characterized by a significant decrease of *Pinus* pollen from 47.4% to 32.8%, and an increase of *Abies*/*Picea*, *Quercus* (E), *Cyclobalanopsis*, *Alnus*, *Betula*, and *Salix*. In this zone, *Tsuga* and *Quercus* (D) pollen reaches their minima of the entire core, whereas herbaceous pollen reaches its maximum of the entire core. Pollen influx values of both arboreal pollen, such as *Pinus*, *Quercus* (E), *Cyclobalanopsis*, *Lithocarpus*/*Castanopsis*, *Alnus*, and *Salix*, and nonarboreal pollen, such as Poaceae, Cyperaceae, Cruciferae, and *Artemisia*, show an upward trend. The total pollen influx values of this zone (2815 grains cm^{-2} a^{-1}) are much lower than zone III, but slightly higher than zone II. The charcoal influx values of each particle size in this zone are as high as zone III or even higher than zone III; especially, the total charcoal influx value at 14 cm (ca. 1980 AD) is 35666 particles cm^{-2} a^{-1}, reaching its maximum value of core HXH-1.

PCA was conducted on pollen percentage data of selected major arboreal pollen types having the averages of pollen percentages for all samples more than 1%. Arboreal pollen types include *Pinus*, *Tsuga*, *Abies*/*Picea*, *Quercus* (D), *Quercus* (E), *Cyclobalanopsis*, *Lithocarpus*/*Castanopsis*, Rosaceae, *Alnus*, *Betula*, *Juglans*, *Salix*. PCA result shows that the first two axes explain 43.29 and 16.7% of total variance in this pollen dataset, respectively (Figure 8). As shown by Figure 8, *Tsuga* and *Pinus* have positive loading on the PCA axis 1, whereas *Lithocarpus*/*Castanopsis, Cyclobalanopsis, Alnus* and *Salix* seize negative loading, significantly separating three pollen zones. PCA axis 1 indicates a process of vegetation succession from vegetation dominated by coniferous forest (zone III) to one dominated by evergreen broadleaved forest (zone I). Zone II reflects a transitional vegetation between above two vegetation types. PCA axis 2 separates coniferous tree pollen types (*Pinus* and *Abies*/*Picea*) from deciduous and evergreen broadleaved tree as well as shrub pollen types (e.g., *Quercus* (E), *Quercus* (D), *Alnus* and Rosaceae), implying changes in minor components of above vegetation types.

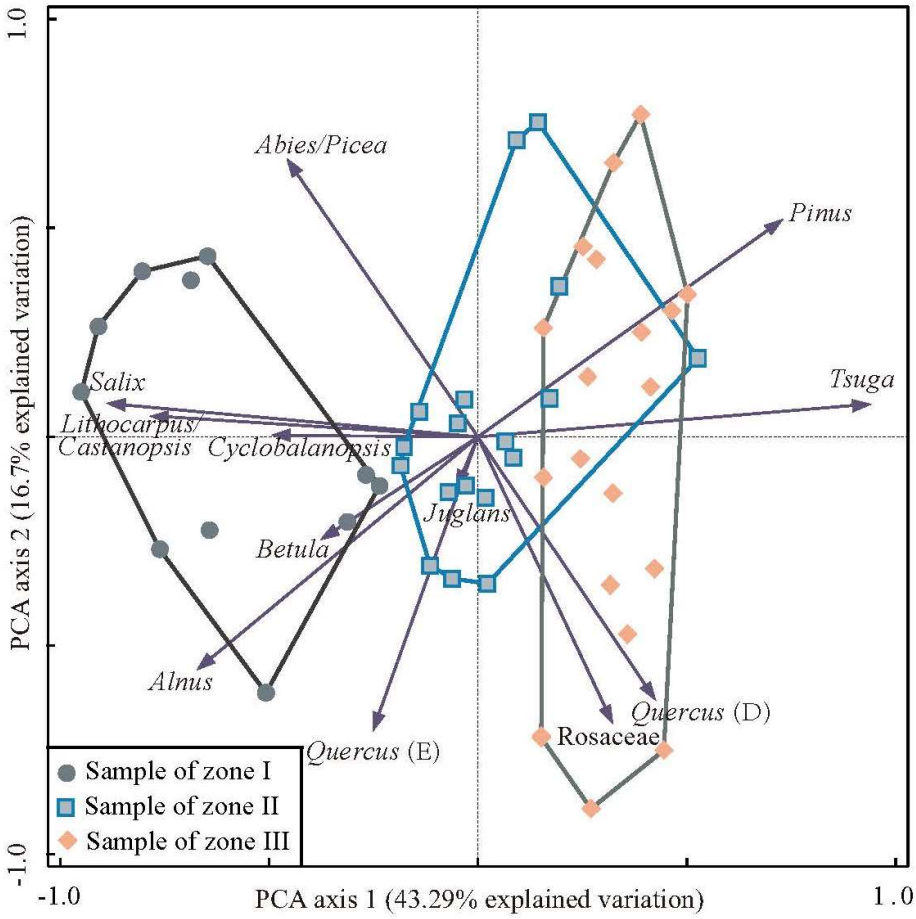


Figure 8. Biplot of PCA on pollen percentage data of twelve arboreal pollen taxa for core HXH-1 from Lake Haixihai. The samples were grouped in terms of pollen zones.

4.4. Vegetation succession and forest fires in the Lake Haixihai catchment

As shown by Figures 6-8, the Lake Haixihai catchment witnessed three-stage of changes in vegetation succession and forest fires during the last 1640 years.

Stage III (380-1180 AD; pollen zone III): Vegetation of this stage in the Lake Haxihai catchment was dominated by coniferous forests, involving mainly pine and hemlock forests accompanied by a few *Abies*/*Picea* trees. Evergreen broadleaved forest was also common in pollen source area. Its upper layer was composed of evergreen broadleaved trees such as *Quercus* (E), *Castanopsis*/*Lithocarpus* and *Cyclobalanopsis*, as well as some deciduous broadleaved trees such as *Quercus* (D), *Alnus, Betula,* and *Juglans.* Its understory shrubs and herbs mainly included Rosaceae, Poaceae, *Artemisia,* and Ranunuculaceae. As a proxy of vegetation density, total pollen influx values show that forests in this stage were the densest in the Lake Haixihai catchment during the last 1640 years. Meanwhile, the abundance of forest elements and forest densities also indicate that vegetation succession of this stage can be divided three sub-stages (corresponding to three pollen subzones). The sub-stage III-2 is distinguished from other two substages by more coniferous trees such as *Pinus* and *Abies*/*Picea*, less deciduous broadleaved trees such as *Alnus* and deciduous *Quercus*, and the highest densities. A significant and abrupt drop in the total pollen influx values, i.e., the forest density, occurred at the transition between substages III-~~1~~ and III-~~2~~. After this transition, forest density never returned as high as that in the substages III-3 and 2. The charcoal influx values show a similar pattern to the total pollen influx values. Substages III-3, 2, and 1 witnessed low, high, and low frequent forest fires, respectively.

Stage II (1180-1770 AD; pollen zone II): In this stage, coniferous forests decreased significantly, especially pine and hemlock forests. More deciduous broadleaved trees, especially *Alnus* and *Juglans*, occurred in the evergreen broadleaved forests. In the catchment of Lake Haixihai, understory herbs of forests, meadows, and/or cultivated plants of Poaceae increased in the relative abundances of vegetation. However, the total pollen influx values show that the vegetation densities of this stage were the lowest over the last 1640 years. ~~Low frequent~~ forest fires occurred at 1180-1770 AD as indicated by low charcoal influx values.

Stage I (1770 AD to the present; pollen zone I): In the vegetation of this period, the relative abundance of coniferous forests continued to decrease significantly, whereas the evergreen broadleaved forests increased markedly. In the coniferous forests, *Tsuga* trees were inclined to appear sporadically, and *Abies*/*Picea* trees were common; in the evergreen broadleaved forests, more evergreen broadleaved trees such as *Quercus* (E), *Lithocarpus*/*Castanopsis*, and *Cyclobalanopsis*, as well as more deciduous broadleaved trees such as *Alnus* and *Salix* were present. The content of herbs was still as high as that in the stage II, and even more in the middle of this stage. The total pollen influx values in this stage were slightly higher than those in stage II but still much lower than those in stage III, implying that the vegetation densities of this stage were still at a low level. This stage can be divided into two substages in terms of a significant increase of *Lithocarpus*/*Castanopsis* and *Salix* trees and a marked decrease of herbaceous Poaceae. The charcoal influx values show that the frequency of forest fires in the substage I-~~1~~ was still as low as that in the stage II, but it sharply increased to be the highest over the last 1640 years in the substage I-1.

5. Discussion

5.1. The soil erosion in the Lake Haixihai catchment during the last 1640 years

The PC1 of six major elements, a proxy of the soil erosion intensity in the lake catchment, revealed that the erosion intensity of the last 1640 years experienced three-phase changes (Figure 9d). This fact was also supported by the lithology of Core HXH1 (Figure 2). Furthermore, the magnetic susceptibility (Figure 9e), another effective proxy of soil erosion [31,51], showed a parallel pattern to that revealed by PC1 scores, implying our reliable interpretation of the PCA result of six major elements.

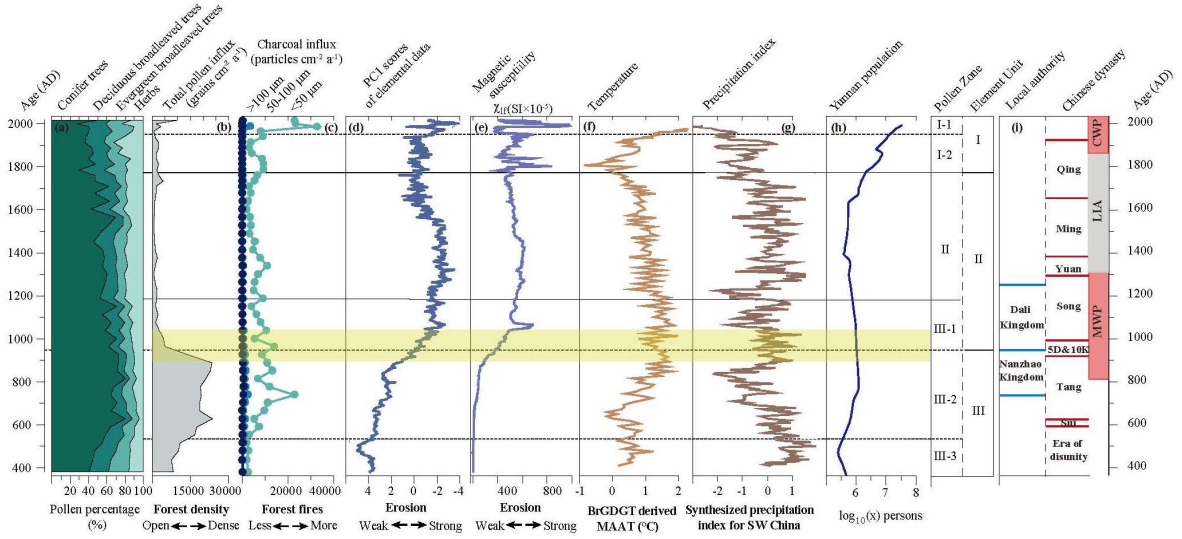


Figure 9. A comparison of vegetation, forest fire, soil erosion intensity in the Lake Haixihai catchment over the last 1640 years with regional temperature and precipitation, population in Yunnan Province. (a) vegetation history represented by abundance of four pollen groups; (b) total pollen influx as a proxy of forest density; (c) charcoal influx as a proxy of forest fire frequency; (d~~-e~~) PC1 scores of element data as a proxy of soil erosion intensity, and magnetic susceptibility (χ_{lf}) as another

proxy of soil erosion intensity; (f) brGDGT-inferred MAAT reconstruction in Tiancai Lake based on the site-specific brGDGT-temperature calibration model [54]; (g) the synthesized precipitation index for southwest China derived from stalagmite $\delta^{18}O$ records at Shenqi cave in southern Sichuan, China [53]; (h) logarithmic (base 10) population of Yunnan Province [58]; (i) local authority and Chinese dynasties. The major transition of vegetation and soil erosion intensity is marked by the yellow bar. The Medieval warm period (MWP) and current warm period (CWP) are marked by red boxes, and little ice age (LIA) is marked by the grey box.

Our results showed that the weakest erosion of the last 1640 years occurred at 380-880 AD when the densest forests occupied the lake catchment (Figure 9b). This period was followed by a major transition of soil erosion intensity from weak to strong erosion at 880-1040 AD. After this major transition, the persistent and strong erosion kept until the present, and it never returned to the erosion conditions as weak as before 880 AD, although it experienced secondary oscillations, especially in period from 1940 AD to nowadays. A pollen record from Lake Erhai suggested that forest clearance occurred as early as 2140 cal. yr. BP, but extensive deforestation probably happened after the end of Tang Dynasty (900 AD) when irrigated technique in agriculture was widely used [9,52]. It is evident that this pollen record supports our result, since the Lake Haixihai catchment is one part in the northwest of Lake Erhai basin.

The above major transition of soil erosion was apparently driven by climate conditions (Figure 9f-g) and anthropogenic forcings (Figure 9h-i). An integrated precipitation record for southwestern China [53] and a brGDGT-inferred MAAT record from Lake Tiancai [54] showed that the Lake Haixihai catchment witnessed a major drought with higher temperature and lower precipitation than those at the present from 700 to 860 AD. Accompanying this major drought were more forest fires. It is evident that this major drought and more forest fires created climatic and vegetational background for this major transition of soil erosion intensity as temperature kept high and precipitation became higher than the present. On the other hand, the establishment of the Nanzhao Kingdom in the Lake Erhai basin and the friendly alliance relation with Tang Dynasty brought population pressure requiring more agricultural land (Figure 9h) [55-57]. At the late period of the Nanzhao Kingdom, the alliance relations with Tang Dynasty and Tubo Dynasty deteriorated and ruptured successively, which resulted in the transfer of the capital as well as the construction and reinforcement of a series of military fortresses such as ancient Cities Taihe (old capital), Yangqiemie (new capital), Shiqiao, Shihe, Longku, Longwei, Dali, Dengchuan, Baixia, Yunnan, and Longyutushan for both offense and defense [56]. These activities led to the beginnings of systematic deforestation [55]. Furthermore, the replacement of Nanzhao Kingdom by Dali Kingdom happened at 930s AD under the political view "Tax relief for grain and welfare corvee labor". This political view of Dali Kingdom unaffectedly resulted in the development of agriculture, thus enhancing the soil erosion.

5.2. Vegetation succession and forest fires driven by both natural and anthropogenic forcings

Our study revealed three-stage of changes in vegetation succession and forest fires during the last 1640 years. As discussed above, vegetation succession and forest fires were also driven by both natural and anthropogenic forcings.

Vegetation at stage III (380-1180 AD) was dominated by coniferous forests and evergreen broadleaved forests. However, this stage can be divided into three substages in terms of forest composition and density. The lake catchment saw more evergreen broadleaved forests and intermediate forest density at the substage III-3, when regional temperature and precipitation were higher than the present (Figure 9f-g). At this substage, the Lake Erhai basin was governed by separate tribes and Yunnan had low population (Figure h-i) [57,58], implying the least impact on vegetation from human activities over the last 1640 years. Less human-induced impact on vegetation at this substage was also revealed by pollen records from Lakes Erhai [9], Tiancai [19], Tengchong Qinghai [21,59,60], Lugu [61] and Xingyun [12] as well as the Beihai wetland [5,62] in Yunnan. The Lake Haixihai

catchment witnessed the densest vegetation consisting of more pine and hemlock forests and less evergreen broadleaved forests at the substage III-2, when both regional temperature and precipitation underwent a process of dropping, lower than the present, and rising to higher than the present although they did not change in completely synchronous way. At this substage, the Lake Erhai basin was governed by separate tribes and Nanzhao Kingdom before and after 738 AD [56]. As mentioned in above section, the Lake Haixihai catchment experienced a major drought at 700-860 AD, and saw more frequent forest fires. It is not unexpected that more forest fires occurred at 700-860 AD since the biofuel accumulation (the densest vegetation) and a major drought should promote the occurrence of forest fires [63]. Overall, our results suggested that the vegetation succession and forest fires were mainly driven by natural forcing, i.e., climate conditions. A significant and abrupt drop in forest density and minor changes in abundance of forest components occurred at the transition between substages III-1 and III-2. After this transition, forest density never returned to the level as high as that in the substages III-3 and 2. This transition of vegetation succession completely coincided the major transition of soil erosion, indicating the same driving forcings affecting both vegetation and soil erosion, i.e., anthropogenic forcings were dominant ones driving vegetation succession and soil erosion in this major transition at 880-1040 AD. Minor changes in abundance of forest components but significant difference in forest density occurred between the substages III-2 and III-1, presumably suggesting that the landscape similar to modern one (Figure 10) was already established approximately as early as ca. 1040 AD.

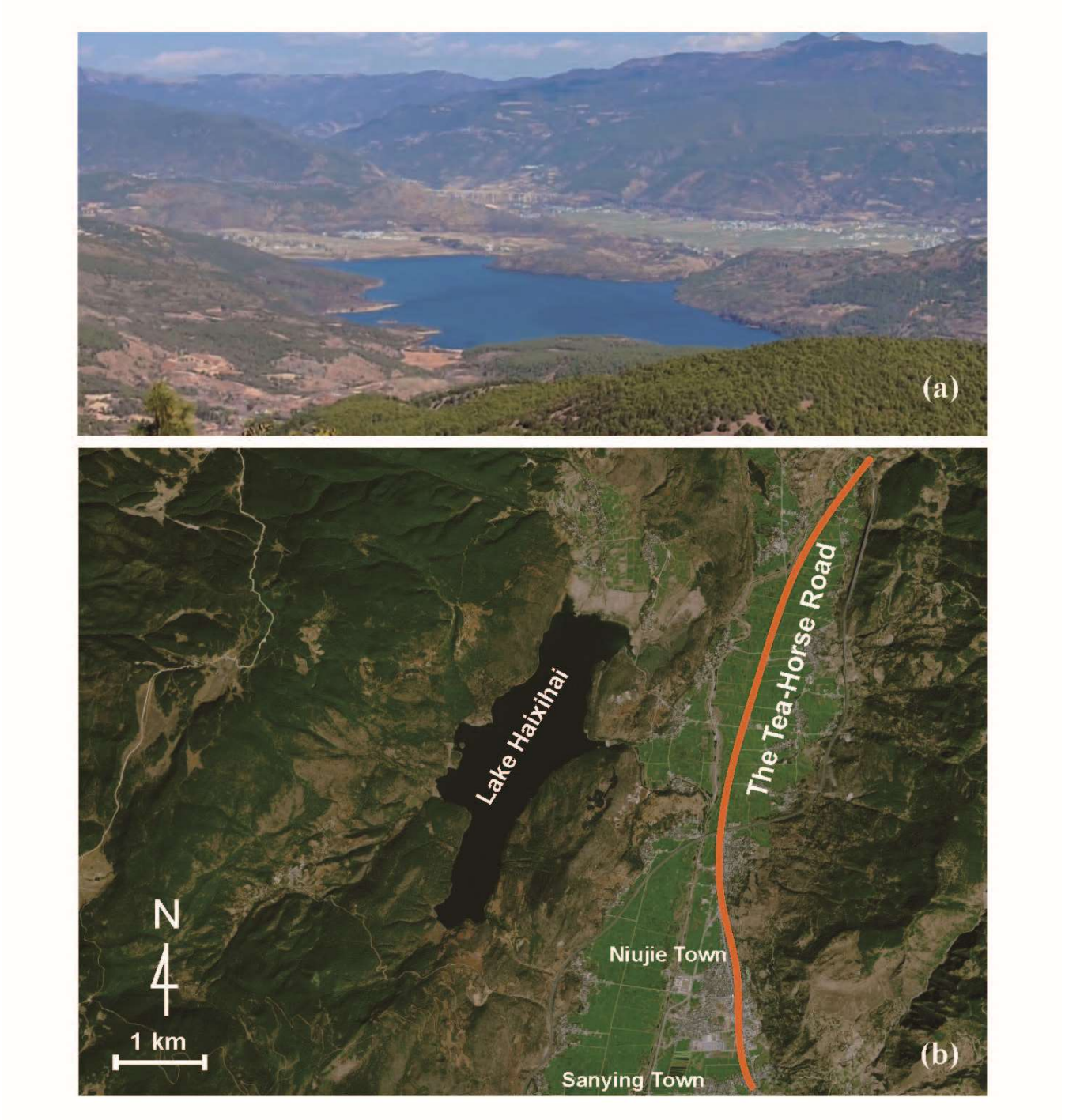


Figure 10. A photo taken from west side of Lake Haixihai showing modern landscapes and vegetation in the lake catchment (a), and a satellite image showing modern land covers including farmlands (light green) as well as towns and the ancient Tea-Horse Road in the lake catchment (b).

Vegetation at stage II (1180-1770 AD) was composed of less pine and hemlock forests as well as more evergreen broadleaved forests and meadows, and had low forest density. At this stage, forest fires were not as common as those in the stage III, vegetation and soil erosion never recovered to the climate-driven levels of the substages III-2 and III-3, although regional temperature and precipitation became higher than the present. The Lake Erhai basin and Yunnan were then governed by Chinese central dynasties. Although population in Yunnan decreased, the Lake Erhai basin as the political and economic center got more population pressure. For example, "In the 15th year of Hongwu in the Ming

Dynasty (1382), the Army General, Mu Ying, was ordered to conquer Yunnan Province. He brought in 200 thousand garrison troops and peasants (mainly people of Han ethnicity) to reclaim land and grow food grain in the areas surrounding Dali and Erhai. The sudden influx of large numbers of people made a great contribution to the economic development of the area, but also brought considerable land pressure and people began to move up to the mountainous areas" [64]. Sanying Town near Lake Haixihai (Figure 10) once was a military camp with a granary as the center of the garrison reclamation in Yuan, Ming and Qing times [65]. Niujie Town near the lake (Figure 10) once was a courier station of the ancient Tea-Horse Road as a millennium southern Silk Roads, it could thus be bustling place [66]. Therefore, the vegetation succession at this stage was still mainly driven by anthropogenic forcings, as suggested by strong soil erosion intensity.

Vegetation at stage I (1770 AD to the present) was dominated by evergreen broadleaved forests and meadows, and had low forest density. At this stage, coniferous forest shrank, forest fires increased, and soil erosion exhibited drastic changes, especially the substage I-1. Climatologically, following the decrease trend of the previous stage, regional temperature dropped to be lower than the present at the end of Little Ice Age, and then rose to be higher than the present in the current warm period; regional precipitation showed a nonlinearly decreasing trend. The strongest soil erosion, the highest frequent forest fires, and low forest density after 1940 AD might be attributed to both climatic conditions and extensive deforestation during the "Great Leap Forward" around 1960 AD [67].

6. Conclusions

Pollen/charcoal and XRF analyses of lacustrine sediments from Lake Haixihai were conducted in this study to reveal the changes of vegetation, forest fire, and soil erosion intensity over the last 1640 years in the lake catchment. We obtained the following four conclusions:

1. PC1 derived from the PCA of six major elements, which were obtained from XRF analysis of lacustrine sediments from Lake Haixihai, is an effective proxy of soil erosion intensity. The weakest erosion of the last 1640 years occurred at 380-880 AD, which was followed by a major transition of soil erosion intensity from weak to strong erosion at 880-1040 AD. The persistent and strong erosion then kept until the present.

2. Pollen analysis of lacustrine sediments from Lake Haixihai revealed that the Lake Haixihai catchment experienced three-stage of vegetation succession over the last 1640 years. The densest forests, which were dominated by pine and hemlock as well as evergreen broadleaved forests, occurred at 380-950 AD. A transition, which was characterized by significant drop in forest density, appeared at 950-1180 AD. After this transition, coniferous forests shrank, evergreen broadleaved forests as well as meadows, understory herbs and/or cultivated plants expanded, but the forest density kept low level until the present.

3. More frequent forest fires occurred at intervals around 700 AD and after 1940 AD. The former was associated with the accumulation of biofuels and a major drought, the latter was driven by climatic conditions and human impacts.

4. Our study suggests that the driving forcings of vegetation, forest fire, and soil erosion were dominated by natural ones at 380-880 AD; at a transition from 880 to 1040 AD, anthropogenic forcings gradually replaced natural ones; and the driving forcings were dominated by anthropogenic forcings after this transition.

Acknowledgements: This research was supported by grants from the National Natural Science Foundation of China (Grant Nos 42177437, 41372191, 42067061), Special Project for Basic Research of Yunnan Province—Key Project (Grant No. 202101AS070006), the Yunnan Project for the Introduction of Advanced Talents (Grant No. 2013HA024). We thank Drs. Wenxiang Zhang and Lingyang Kong, Mr. Qiushi Liang, Lu Wang, Peng Wang, Guofu Zhang, and Tao Zhang for their help in field trip.

References

[1] Turney, C.S.M.; McGregor, H.V.; Francus, P.; Abram, N.; Evans, M.N.; Goosse, H.; von Gunten, L.; Kaufman, D.; Linderholm, H.; Loutre, M.F.; Neukom, R. Introduction to the special issue "Climate of the past 2000 years: regional and trans-regional syntheses". *Clim. Past* **2019**, 15, 611-615.

[2] Marlon, J.R.; Bartlein, P.J.; Carcaillet, C.; Gavin, D.G.; Harrison, S.P.; Higuera, P.E.; Joos, F.; Power, M.J.; Prentice, I.C. Climate and human influences on global biomass burning over the past two millennia. *Nat. Geosci.* **2008**, 1, 697-702.

[3] Yan M.; Wang Z.; Kaplan J.O.; Liu J.; Min S.; Wang S. Comparison between reconstructions of global anthropogenic land cover change over past two millennia. *Chinese Geogr. Sci.* **2013**, 23, 131-146.

[4] Cao, X.Y.; Tian, F.; Herzschuh, U.; Ni, J.; Xu Q.H.; Li, W.J.; Zhang, Y.R.; Luo M.Y.; Chen, F.H. Human activities have reduced plant diversity in eastern China over the last two millennia. *Global Change Biol.* **2022**, 28, 4962-4976.

[5] Wang, Y.B.; Xie, Y.; Liu, X.Q.; Shen, J.; Wang, Y.; Li, Z. Climate and human induced 2000-year vegetation diversity change in Yunnan, southwestern China. *The Holocene* **2022**, 32, 1327-1339.

[6] López-Pujol, J.; Zhang, F.M.; Ge, S. Plant biodiversity in China: Richly varied, endangered, and in need of conservation. *Biodivers. Conserv.* **2006**, 15, 3983–4026.

[7] Chen, C.J; Huang, R; Yuan, D.X.; Zhang, J.; Cheng, H.; Ning, Y.F.; Yu, T.L.; Shen, C.C.; Edwards, R. L.; Long, X.Y.; Wang, T.; Xiao, S.Y.; Wu, Y.; Liu, Z.Q.; Li, T.Y.; Li, J.Y. Karst hydrological changes during the Late-Holocene in Southwestern China. *Quat. Sci. Rev.* **2021**, 258, 106865.

[8] Zheng, Q.; Zhang, H.C.; Ming, Q.Z.; Chang, F.Q.; Meng, H.W.; Zhang, W.X.; Liu, M.Z.; Shen, C.M. Vegetational and Environmental Changes since 15ka BP Recorded by Lake Lugu in the Southwest Monsoon Domain Region. *Quat. Sci.* **2014**, 34, 1314-1322. (In Chinese)

[9] Shen, J.; Jones, R.T.; Yang, X.D.; Dearing, J.A.; Wang, S.M. The Holocene vegetation history of Lake Erhai, Yunnan province southwestern China: the role of climate and human forcing. *The Holocene* **2006**, 16, 265-277.

[10] Xiao, X.Y.; Haberle, S.G.; Li, Y.L.; Liu, E.F.; Shen, J.; Zhang, E.L.; Yin, J.J.; Wang, S.M. Evidence of Holocene climatic change and human impact in northwestern Yunnan Province: High-resolution pollen and charcoal records from Chenghai Lake, southwestern China. *The Holocene* **2018**, 28, 129-137.

[11] Liu, X; Wu, Y.; Jiang, Z.; Long, R.; Li, B.; Brenner, M.; Whitmore, T.J.; Engstrom, D.R.; Moore, A. *Paleoliminological studies on the limestone district in central Yunnan, China*. Yunnan Science and Technology Press: Kunming, China, 1993**.** (In Chinese)

[12] Chen, F.H.; Chen, X.M.; Chen, J.H.; Zhou, A.F.; Wu, D.; Tang, L.Y.; Zhang, X.J.; Huang, X.Z.; Yu, J.Q. Holocene vegetation history, precipitation changes and Indian Summer Monsoon evolution documented from sediments of Xingyun Lake, south-west China. *J. Quat. Sci.* **2014**, 29, 661-674.

[13] Sun, Q.F.; Shen, C.M.; Wang, M.; Meng, H.W.; Zhang, H.C. Pollen/charcoal record over the past 13300 years from Fuxian Lake in the Yunnan-Guizhou Plateau. *Acta Palaeontol. Sin.* **2018**, 57, 249-259. (In Chinese)

[14] Xiao, X.Y.; Yao, A.; Hillman, A.; Shen, J.; Haberle, S.G. Vegetation, climate and human impact since 20 ka in central Yunnan province based on high-resolution pollen and charcoal records from Dianchi, southwestern China. *Quat. Sci. Rev.* **2020**, 236, 106297.

[15] Wang, M.; Meng, H.W.; Huang, L.P.; Sun, Q.F.; Zhang, H.C.; Shen, C.M. Vegetation succession and forest fires over the past 13000 years in the catchment of Yangzong Lake, Yunnan. *Quat. Sci.* **2020**, 40, 175-189. (In Chinese)

[16] Yuan, Z.J.; Wu, D.; Niu, L.L.; Ma, X.Y.; Li, Y.M.; Hillman, A.L.; Abbott, M.B.; Zhou, A.F. Contrasting ecosystem responses to climatic events and human activity revealed by a sedimentary record from Lake Yilong, southwestern China. *Sci. Total Environ*. **2021**, 783, 146922.

[17] Jacobson, G.L.; Bradshaw, R.H.W. The selection of sites for paleovegetational studies. *Quat. Res.* **1981**, 16, 80-96.

[18] Lin, S.M.; Qiao, Y.L.; Walker, D. Late Pleistocene and Holocene vegetation history at Xi Hu, Er Yuan, Yunnan Province, southwest China. *J. Biogeogr.* **1986**, 13, 419-440.

[19] Xiao, X.Y.; Haberle, S.G.; Shen, J.; Yang, X.D.; Yong, H.; Zhang, E.L.; Wang, S.M. Latest Pleistocene and Holocene vegetation and climate history inferred from an alpine lacustrine record, northwestern Yunnan Province, south-western China. *Quat. Sci. Rev.* **2014**, 86, 35-48.

[20] Jiang, W.Y.; Leroy, S.A.; Yang, S.L.; Zhang, E.L.; Wang, L.; Yang, X.X.; Rioual, P. Synchronous strengthening of the Indian and East Asian monsoons in response to global warming since the last deglaciation. *Geophys. Res. Lett.* **2019**, 46, 3944-3952.

[21] Xiao, X.Y.; Haberle, S.G.; Shen, J.; Xue, B.; Burrows, M.; Wang, S.M. Postglacial fire history and interactions with vegetation and climate in southwestern Yunnan Province of China. *Clim. Past* **2017**, 13, 613-627.

[22] Yang, L.; Li, H. (ed.). *Wetlands of Yunnan*; China Forestry Publishing House: Beijing, China, 2010. (In Chinese)

[23] Water conservancy and electricity Bureau of Eryuan County (ed.). *Water Conservancy Records of Eryuan County;* Yunnan University Press: Kunming, China, 1995. (In Chinese)

[24] Wu, Z.; Zhu, Y.; Jiang, H. (eds.). *Yunnan Vegetation;* Science Press: Beijing, China, 1987. (In Chinese)

[25] Zhang, P.; Zhang, J.; Li, J.Y.; Xue, Y.F.; Li, Y.C. Vertical distribution pattern of vegetation on the east and west slopes of Cangshan Mountain in Dali. *J. Zhejiang A & F University.* **2022**, 39, 68-75.

[26] Editorial Board of Vegetation Map of China, Chinese Academy of Sciences. *Vegetation Atlas of China*; Science Press: Beijing, China, 2001. (In Chinese)

[27] Lei, G.L.; Zhang, H.C.; Chang, F.Q.; Zhu, Y.; Li, C.H.; Xie, X.; Lei, T.B.; Zhang, W.X.; Pu, Y. Comparison and correction of element measurements in lacustrine sediments using X-ray fluorescence core-scanning with ICP-OES method: A case study of Zigetang Co. *J. Lake Sci.* **2011**, 23, 287-294. (In Chinese)

[28] Arz, H.W.; Patzold, J.; Muller, P.J. Influence of Northern Hemisphere climate and global sea level rise on the restricted Red Sea marine environment during termination I. *Paleoceanography* **2003**, 18, 1053.

[29] Nizou, J.; Hanebuth, T.J.J.; Vogt, C. Deciphering signals of late Holocene fluvial and aeolian supply from a shelf sediment depocenter off Senegal (north-west Africa). *J. Quat. Sci.* **2011**, 26, 411-421.

[30] Zhang, X.N; Zhang, C.; Wu, D.; Zhou, A.F. Element geochemical characteristics of lake sediments measured by X-ray Fluorescence (XRF) core scanner in Northwest China. *Mar. Geol. Quat. Geol.* **2015**, 35, 163-174. (In Chinese)

[31] Chang, J.; Zhang, E.L.; Liu, E.F.; Sun, W.W.; Langdon, P.G.; Shulmeister, J. A 2500-year climate and environmental record inferred from subfossil chironomids from Lugu Lake, southwestern China. *Hydrobiologia* **2018**, 811, 193-206.

[32] Turner, J.N.; Holmes, N.; Davis, S.R.; Leng, M.J.; Langdon, C.; Scaife, R.G. A multiproxy (micro-XRF, pollen, chironomid and stable isotope) lake sediment record for the Lateglacial to Holocene transition from Thomastown Bog, Ireland. *J. Quat. Sci.* **2015**, 30, 514-528.

[33] Haug, G.H.; Hughen, K.A.; Sigman, D.M.; Peterson, L.C.; Rohl, U. Southward migration of the intertropical convergence zone through the Holocene. *Science* **2001**, 293, 1304-1308.

[34] Shen, J.; Wu, X.D.; Zhang, Z.H.; Gong, W.M.; He, T.; Xu, X.M.; Dong, H.L. Ti content in Huguangyan maar lake sediment as a proxy for monsoon-induced vegetation density in the Holocene. *Geophys. Res. Lett.* **2013**, 40, 5757-5763.

[35] Zhang, E.L.; Zhao, C.; Xue, B.; Liu, Z.H.; Yu, Z.C.; Chen, R.; Shen, J. Millennial-scale hydroclimate variations in southwest China linked to tropical Indian Ocean since the last glacial maximum. *Geology* **2017**, 45, 435-438.

[36] Kern, O.A.; Koutsodendris, A.; Machtle, B.; Christanis, K.; Schukraft, G.; Scholz, C.; Kotthoff, U.; Pross, J. XRF core scanning yields reliable semiquantitative data on the elemental composition of highly organic-rich sediments: Evidence from the Furamoos peat bog (Southern Germany). *Sci. Total Environ*. **2019**, 697, 110-134.

[37] Longman, J.; Veres, D.; Wennrich, V. Utilisation of XRF core scanning on peat and other highly organic sediments. *Quat. Int.* **2019**, 514, 85-96.

[38] Yang, H.; Zeng, M.X.; Peng, H.J.; Li, K.; Li, F.Q.; Zhu, L.D.; Deng, B.L.; Liao, M.N.; Ni, J. Application of XRF core scanning method in Late Holocene environment change study derived from a peat core from southwestern Guizhou, Southwestern China. *Quat. Sci.* **2020**, 40, 1154-1169. (In Chinese)

[39] Faegri, K.; Iversen, J. *Textbook of Pollen Analysis;* Macmillan: New York, 1975.

[40] Stockmarr, J. Tablets with spores used in absolute pollen analysis. *Pollen et Spores*. **1971**, 13, 615-621.

[41] Davis, M.B.; Brubaker, L.B.; Webb, T.I. Calibration of pollen influx; In: Birks, H.J.B., West, R.G. (eds.), *Quaternary Plant Ecology*; Blackwell Oxford, 1972, 9-25.

[42] Mehringer, P.J.; Blinman, E.; Petersen, K.L. Pollen influx and volcanic ash: The pollen content of Mazama and Glacier Peak ashes reveals details of their depositional chronologies. *Science* **1977**, 198, 257-261.

[43] Birks, H.J.B.; Birks, H.H. *Quaternary Palaeoecology*; Edward Arnold: London, 1980.

[44] Li, Y.Y.; Hou, S.F.; Zhao, P.F. Comparison of different quantification methods for microfossil charcoal concentration and the implication for human activities. *Quat. Sci.* **2010**, 30, 356-363. (In Chinese)

[45] Grimm, E.C. CONISS: A FORTRAN 77 program for stratigraphically constrained cluster analysis by the method of incremental sum of squares. *Comput Geosci.* **1987**, 13, 13-35.

[46] Reimer, P.J.; Austin, W.E N; Bard, E.; Bayliss, A.; Blackwell, P.G; Ramsey, C.B; Butzin M.; Cheng H.; Edwards R.L.; Friedrich M.; et al. The IntCal20 Northern Hemisphere Radiocarbon Age Calibration Curve (0–55 cal kBP). *Radiocarbon* **2020**, 62, 725-757.

[47] Quan, H.; Barbetti, M.; Rakowski, A.Z. Atmospheric radiocarbon for the period 1950-2010. *Radiocarbon* **2013**, 55, 2059-2072.

[48] Reimer, P.J.; Bard, E.; Bayliss, A.; Beck, J.W.; Staff, R.A. IntCal13 and Marine13 radiocarbon age calibration curves 0-50,000 years cal BP. *Radiocarbon* **2013**, 55, 1869-1887.

[49] Wang, J.Y.; Chen, G.J.; Kang, W.G.; Hu, K.; Wang, L. Impoundment intensity determines temporal patterns of hydrological fluctuation, carbon cycling and algal succession in a dammed lake of Southwest China. *Water Res.* **2018**, 148, 162-175.

[50] Blaauw, M.; Christen, J.A. Flexible paleoclimate age-depth models using an autoregressive gamma process. *Bayesian Anal*. **2011**, 6, 457-474.

[51] Oldfield, F.; Wake, R.; Boyle, J.; Jones, R.; Nolan, S.; Gibbs, Z.; Appleby, P.; Fisher, E.; Wolff, G. The late-Holocene history of Gormire Lake (NE England) and its catchment: a multiproxy reconstruction of past human impact. *The Holocene* **2003**, 13, 677-690.

[52] Yang, X.D.; Shen, J.; Jones, R.T.; Wang, S.M.; Tong, G.B.; Zhang, Z.K. Pollen evidence of early human activities in Erhai basin, Yunnan Province. *Chinese Sci Bull.* **2005**, 50, 569-577.

[53] Tan, L.C.; Cai, Y.J.; Cheng, H.; Edwards, L.R.; Lan, J.H.; Zhang, H.W.; Li, D.; Ma, L.; Zhao, P.P.; Gao, Y.L. High resolution monsoon precipitation changes on southeastern Tibetan Plateau over the past 2300 years. *Quat. Sci. Rev.* **2018**, 195, 122-132.

[54] Feng, X.P.; Zhao, C.; Andrea, W.J.D.; Liang, J.; Zhou, A.F.; Shen, J. Temperature fluctuations during the Common Era in subtropical southwestern China inferred from brGDGTs in a remote alpine lake. *Earth Planet Sci. Lett.* **2019**, 510, 26-36.

[55] Elvin, M.; Crook, D.S.; Shen, J.; Jones, R.T. Dearing, J.A. The impact of clearance and irrigation on the environment in the Lake Erhai catchment from the ninth to the nineteenth century. *East Asian History* **2002**, 23, 1-60.

[56] Zhang, Z.Q. *The ancient civilization of Erhai region: Period of Nanzhao-Dali Kingdoms*; Yunnan Education Publishing House: Kunming, China, 2010. (In Chinese).

[57] Zhang, Z.Q. *The ancient civilization of Erhai region: Separate tribal governance periods*; Yunnan Education Publishing House: Kunming, China, 2010. (In Chinese).

[58] Zhao, W.L.; Xie, S.J. *Population History of China*; People's Press: Beijing, China, 1988. (In Chinese)

[59] Xiao, X.Y.; Shen, J.; Haberle, S.G.; Han, Y.; Xue, B.; Zhang, E.L.; Wang, S.M.; Tong, G.B. Vegetation, fire, and climate history during the last 18 500 cal a BP in south-western Yunnan Province, China. *J. Quat. Sci.* **2015**, 30, 859-869.

[60] Yang, Y.P.; Zhang, H.C.; Chang, F.Q.; Meng, H.W.; Pan, A.D.; Zheng, Z.; Xiang, R. Vegetation and climate history inferred from a Qinghai Crater Lake pollen record from Tengchong, southwestern China. *Palaeogeogr Palaeoclimatol Palaeoecol.* **2016**, 461, 1-11.

[61] Wang, Q.; Yang, X.D.; Anderson, N.J.; Dong, X.H. Direct versus indirect climate controls on Holocene diatom assemblages in a sub-tropical deep, alpine lake (Lugu Hu, Yunnan, SW China). *Quat. Res.* **2016**, 86, 1-12.

[62] Xie, Y.; Wang, Y.B.; Liu, X.Q.; Shen, J.; Wang, Y. Increasing human activities during the past 2,100 years in southwest China inferred from a fossil pollen record. *Veg. Hist. Archeaobot.* **2021**, 30, 477-488.

[63] Belcher, C.M.; Collinson, M.E.; Scott, A.C. A 450-Million-Year record of fire. In Belcher C M. (eds). *Fire phenomena*

in the earth system-an interdisciplinary approach to fire science. Manhattan: John Wiley and Sons. 2013, 229-249.

[64] Xu, A.; Yang, L.E.; Yang, W.; Hillman, A.L. Resilience of the human-water system at the southern Silk Road: a case study of the northern catchment of Erhai Lake, China (1382–1912). In: Yang, L.E.; Bork, H.R.; Fang, X.Q.; Mischke, S. (eds), *Socio-Environmental Dynamics along the Historical Silk Road*, Springer OPEN, 2019, 325-358.

[65] Liu, L.P. *National governance in Erhai Area and the identity to Bai People in Ming and Qing Dynasties*. Dissertation, Fudan University: Shanghai, China. 2013.

[66] Li, X. *Tea-Horse Road: from the Hengduan Mountains to the Tibetan Plateau*; Qinghai People's Publishing House: Qinghai, China, 2021.

[67] Dali Bai Autonomous Prefecture Forestry Bureau (ed.). *Forestry gazette*. Yunnan Nationalities Publishing House: Kunming, China, 1993.